ELSEVIER

International Journal of Pressure Vessels and Piping 76 (1999) 685–692

INTERNATIONAL JOURNAL OF
Pressure Vessels and Piping

www.elsevier.com/locate/ijpvp

Failure of a threaded pressurized vessel

L.J. Perry[a], E.S. Folias[b,*]

[a]*Quartzdyne, Inc., 1020 Atherton Drive, Salt Lake City, UT 84123 USA*
[b]*Department of Mechanical Engineering, University of Utah, Salt Lake City, UT 84112 USA*

Received 19 February 1999; accepted 15 April 1999

Abstract

A fracture mechanics analysis of a threaded pressure vessel, which has been welded to a plug of similar material is presented. Owing to the presence of threads (circumferential notches) in a pressure vessel, premature fracture may occur due to the propagation of a crack nucleating from the thread root. In order to determine the internal pressure, which induces this fast fracture, a semi-analytical approach is used which combines both linear elastic fracture mechanics and finite element analysis. An estimation of the axial stress required to propagate the crack is obtained from the fracture mechanics approach, using the far-field axial stress in the threaded region recovered from a finite element analysis. Moreover, experimental evidence substantiates the validity of this type of composite analytical approach, by confirming both the rupture pressure and the residual hoop strain after fracture.

Keywords: Cylindrical vessel; Crack; Cracked thread; Thick vessel; Fracture

1. Introduction

In oilfield pressure gauge designs, the pressure-bearing vessel being threaded and then welded to a mating part is a common practice. O-rings are often employed to retain pressure in temporary applications, but in a permanent installation, a weld between parts is generally the rule, for reasons of reliability.

The presence of threads within the vessel is usually ignored, and the design of a thick-walled pressure-bearing vessel relies on simple thick-walled pressure vessel calculations (i.e. the Lamé solution applying for internal pressure [1]). Moreover, end effects are usually ignored. The theory of maximum shear stress gives an estimate of the pressure required to initiate yielding on the internal surface [2]. This general approach neglects to account for the axial stresses arising from the nonconstrained ends of the pressure housing, as well as ignores the presence of threads, sharp interior angles, and other stress risers.

2. Method of approach

Consider a pressure vessel, which has been threaded, and subsequently welded to a plug of same or similar material. Internal pressure applied to the vessel induces hoop, radial, bending, as well as axial stresses. It is theorized that when the axial stresses are sufficiently large, this will cause the nucleation and propagation of a crack from the root of one of the threads, as portrayed by Detail ① in Fig. 1.

In order to determine the required pressure that may cause the vessel to fracture, linear elastic fracture mechanics (LEFM) will be employed. By utilizing the plane strain fracture toughness for the material, the theoretical far-field stress can be estimated, which will then be assigned as the axial stress adjacent to the root of the thread (but not directly at the thread root).

The pressure required to generate the axial (far-field) stresses comparable to those obtained from the LEFM method will be determined utilizing a nonlinear finite element analysis (FEA) package. This pressure should theoretically be sufficient to fracture the vessel near one of the thread roots. The method of approach is illustrated in Fig. 2.

As experimental proof of this method, rupture pressures will also be obtained from actual tests carried out on specimen gauges of the same material. A direct comparison between the experimental and theoretical values of the critical pressures required to rupture the vessel will serve as a confirmation of the validity of this approach. Further confidence in the FEA stress results will be confirmed by comparing the FEA and the experimental hoop strains.

* Corresponding author. Tel.: + 1-801-581-6851; fax: + 1-801-581-4148.

0308-0161/99/$ - see front matter
PII: S0308-0161(99)00036-8

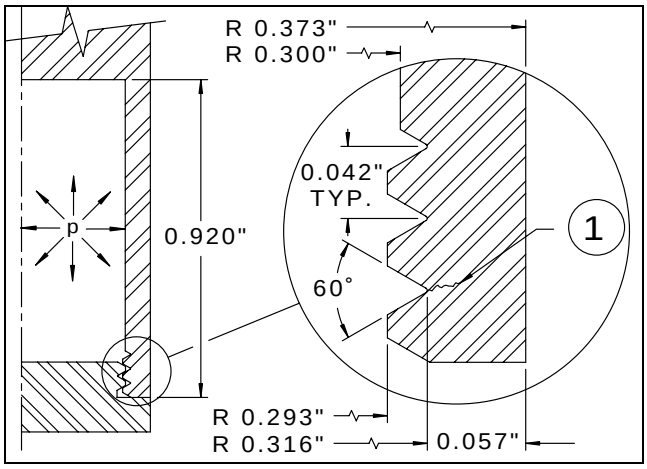

Fig. 1. Threaded pressure vessel.

3. Theoretical background

3.1. Fracture mechanics—geometry considerations

The classic theory of linear elastic fracture mechanics involves a through-thickness crack of length $2a$ in an infinite plate [3]. The mode I stress intensity factor, K_I, is a measure of a material's ability to withstand the propagation of a crack. The generalized stress intensity factor for various structures is given as:

$$K_I = \sigma\sqrt{\pi a}\prod_{i=1}^{n} f_i, \tag{1}$$

where f_i represent multiple geometry correction factors accounting for the boundary conditions, local and global geometry, as well as loading variations. Invoking the theory of fracture mechanics, the failure of the structure occurs when the stress intensity factor reaches the critical value of the fracture toughness, K_{Ic}.

For the particular pressure vessel being analyzed, two geometry correction factors may be applied: the first correction factor accounts for the presence of the internal threads in the vessel, and the second correction factor accounts for the cylindrical vessel geometry.

First, consider Fig. 3, where a 60° notch has been rendered as an edge crack. The stress near a crack tip nominally varies with $r^{-0.5}$. By rendering the 60° notch as an edge crack, the stress field near the notch tip closely approximates that of a crack tip [4], varying with $r^{-0.488}$. Thus, approximating the 60° notch as an edge crack leads to a slightly conservative value, yet nonetheless approximately equivalent. Moreover, once a crack has fatigued itself at the root of the notch, then the conditions will be exact.

Therefore, assuming that a thread (i.e. notch) within a pressure vessel may be approximated by a crack, the first correction factor, f_1, is given by Broek [5]

$$f_1 = \frac{1}{\sqrt{\pi}}\left[1.99 - 0.41\frac{a}{w} + 18.7\left(\frac{a}{w}\right)^2 - 38.48\left(\frac{a}{w}\right)^3 + 53.85\left(\frac{a}{w}\right)^4\right]. \tag{2}$$

For the pressure vessel under investigation (see Fig. 1), the crack length a is the distance from the thread crest to thread

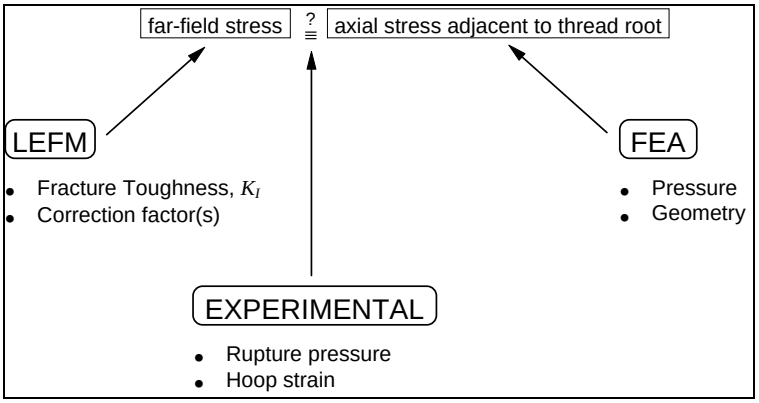

Fig. 2. Solution method flow diagram.

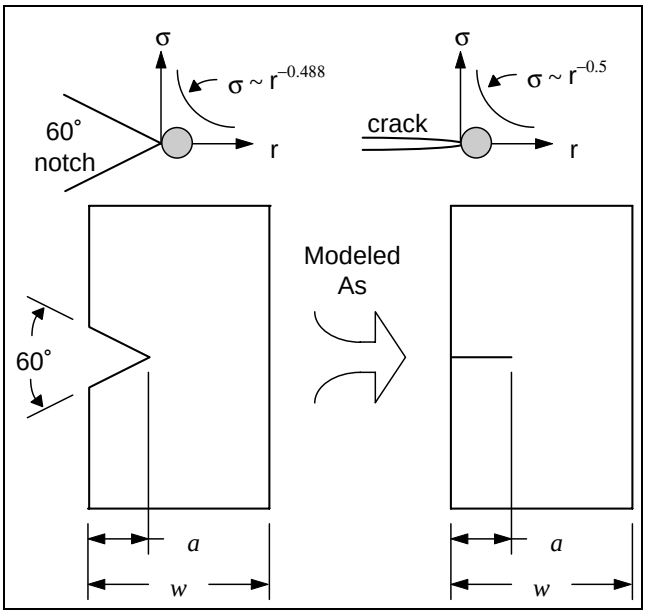

Fig. 3. Modeling an edge notch as an edge crack.

root (0.023 in.), and the thickness w is the pressure vessel wall thickness (0.080 in.). Following this correction, a value of 1.620 is obtained for f_1.

The second geometry correction arises from the fact that the vessel is curved, and is not a flat plate. This correction for a cylindrical curvature is given by Folias [6], i.e.

$$f_2 = \sqrt{1 + \frac{\pi\lambda^2}{64}}, \qquad \lambda^2 = \sqrt{12(1-\nu^2)}\,\frac{a^2}{Rh}. \tag{3}$$

For the pressure vessel being studied, i.e. the crack length $2a$ is one full circumferential length of the thread (1.985 in.), R is the mid-wall radius (0.333 in.), ν is Poisson's ratio (0.29), and h is the wall thickness (0.080 in.). Following this correction, a value of 2.650 is obtained for f_2.

Determining the plane strain fracture toughness, K_{Ic}, for a material is easily obtained by using a compact tension specimen in conjunction with proper testing procedures as outlined in ASTM E399 or ASTM E813. However, in the event that the specimen thickness is smaller than the prescribed thickness for plane strain (h_c), fracture toughness values will vary inversely with thickness, as shown in Fig. 4. Such is the case with the present vessel. Owing to the fact that the plastic zone spreads through the entire wall thickness prior to rupture, the material is actually in a state of triaxial stress, which generally suggests a higher fracture toughness value [7].

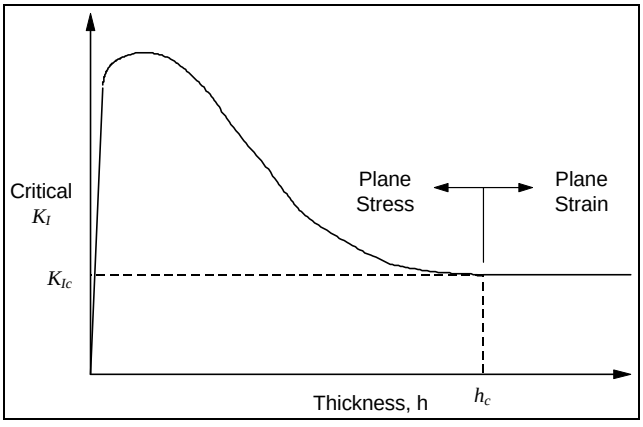

Fig. 4. K_I dependence on specimen thickness.

3.2. Fracture mechanics—material processing considerations

Being one of the popular nickel superalloys, Inconel 718 is a material of choice for many nuclear and oilfield applications. As a precipitation-hardening alloy, it may be hardened for maximum strength or for moderate strength with added resistance to stress corrosion cracking. The heat treatment applied to all Inconel 718 specimens presented in this paper, requires a single aging step following a high temperature solution anneal, and is defined as a modified heat treatment (MHT): Solution anneal at 1093°C (2000°F) for 1 h. Water quench to room temperature. Age at 718°C (1325°F) for 8 h. Air cool to room temperature.

The disadvantage of choosing a nonstandard heat treatment is the lack of available information about material tests and properties. Ideally, fracture toughness tests should be conducted on a material, which has been directly processed, as it will be used during manufacture. Unfortunately, this was not done for specimens receiving the MHT. Nonetheless, it is possible to obtain conservative fracture toughness values for a similar heat treatment. Plane strain fracture toughness values are available for the following conventional heat treatment (CHT): Solution anneal at 1093°C

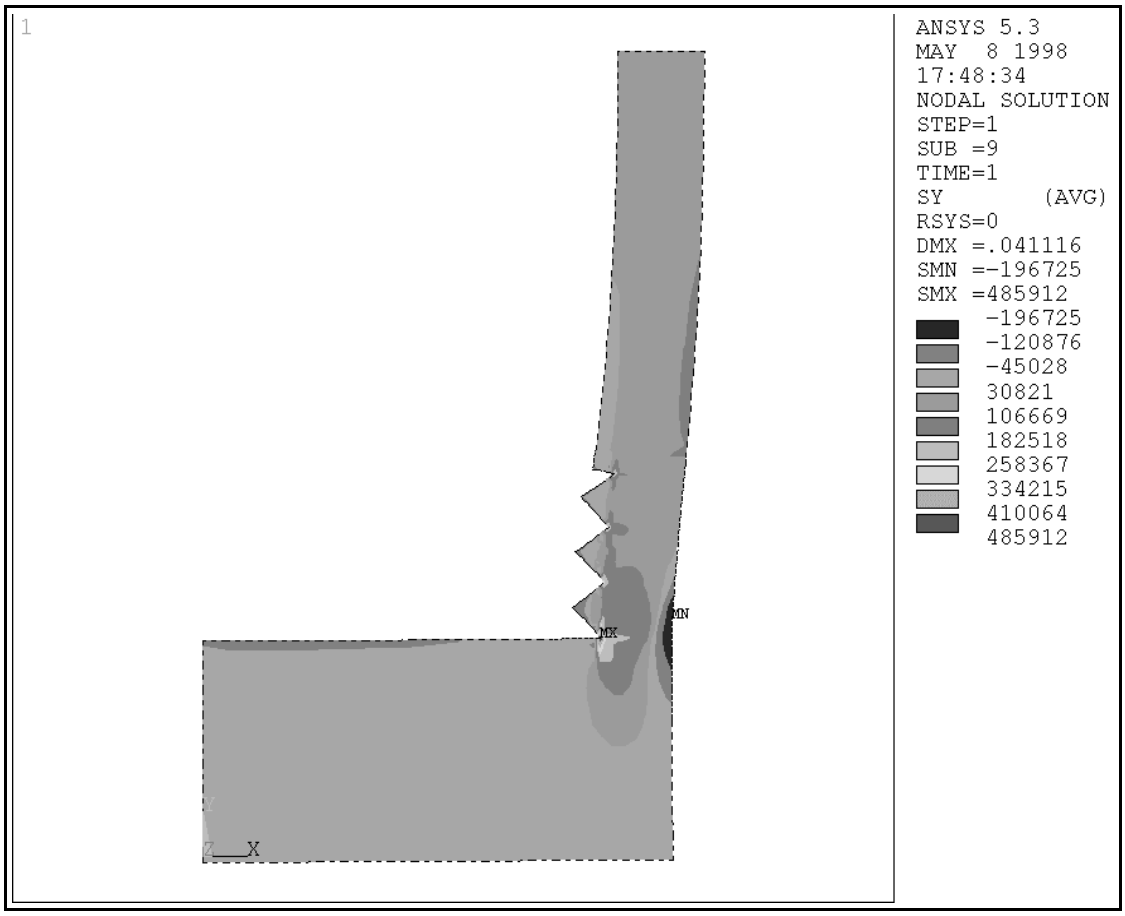

Fig. 5. Axial stress plot of ANSYS model (entire vessel).

(2000°F) for 1 h. Furnace cool at 38°C/h to 718°C (1325°F). Age at 718°C (1325°F) for 4 h. Furnace cool at 38°C/h to 621°C (1150°F). Age at 621°C (1150°F) for 16 h. Air cool to room temperature.

Although this CHT differs from the MHT, the fracture toughness values from the CHT do provide conservative estimates. Inconel 718, which has been aged according to the MHT, will actually have a larger plane strain fracture toughness value, due to the fact that the MHT involves a single age, while the CHT prescribes a double age [8]. Tests [9,10] have indicated that the plane strain fracture toughness for CHT-aged Inconel 718 is approximately 160 ± 40 ksi$\sqrt{\text{in}}$.

There are two reasons to suspect that the fracture toughness value will be larger than the reported value of 160 ksi$\sqrt{\text{in}}$.: (1) the geometry of the pressure vessel indicates a triaxial stress state, not plane strain and (2) the MHT employed for the specimens yields lower tensile and yield strengths, but increased fracture toughness values over the CHT method. For these reasons, analytical calculations will use three fracture toughness values moderately larger (by approximately 6–18%) than the 160 ksi$\sqrt{\text{in}}$. Therefore, by rearranging Eq. (1), and then calculating the far-field stress from the fracture toughness values of 170, 180, and 190 ksi$\sqrt{\text{in}}$. produces

$$\sigma = \frac{K_I}{\sqrt{\pi a} f_1 f_2} = \frac{170 \text{ ksi}\sqrt{in.}}{\sqrt{\pi(0.023)}(1.62)(2.65)} = 147.3 \text{ ksi}$$

$$= \frac{180 \text{ ksi}\sqrt{\text{in.}}}{\sqrt{\pi(0.023)}(1.62)(2.65)} = 156.0 \text{ ksi}$$

$$= \frac{190 \text{ ksi}\sqrt{\text{in.}}}{\sqrt{\pi(0.023)}(1.62)(2.65)} = 164.6 \text{ ksi.} \quad (4)$$

3.3. Finite element analysis procedures

In order to estimate the actual stress state near the threads in the pressure vessel, a finite element (FE) approach was taken. It was desired that the FE model would produce a radial deflection accurately close to that encountered in the experimental phase. If the deflection of the FE model resembled the experimental deflection, it was felt that the stress state, particularly the axial stress, near the root of threads in the pressure housing could be compared to the far-field stress calculated from the fracture mechanics approach.

As a starting point, a linear elastic approach was taken.

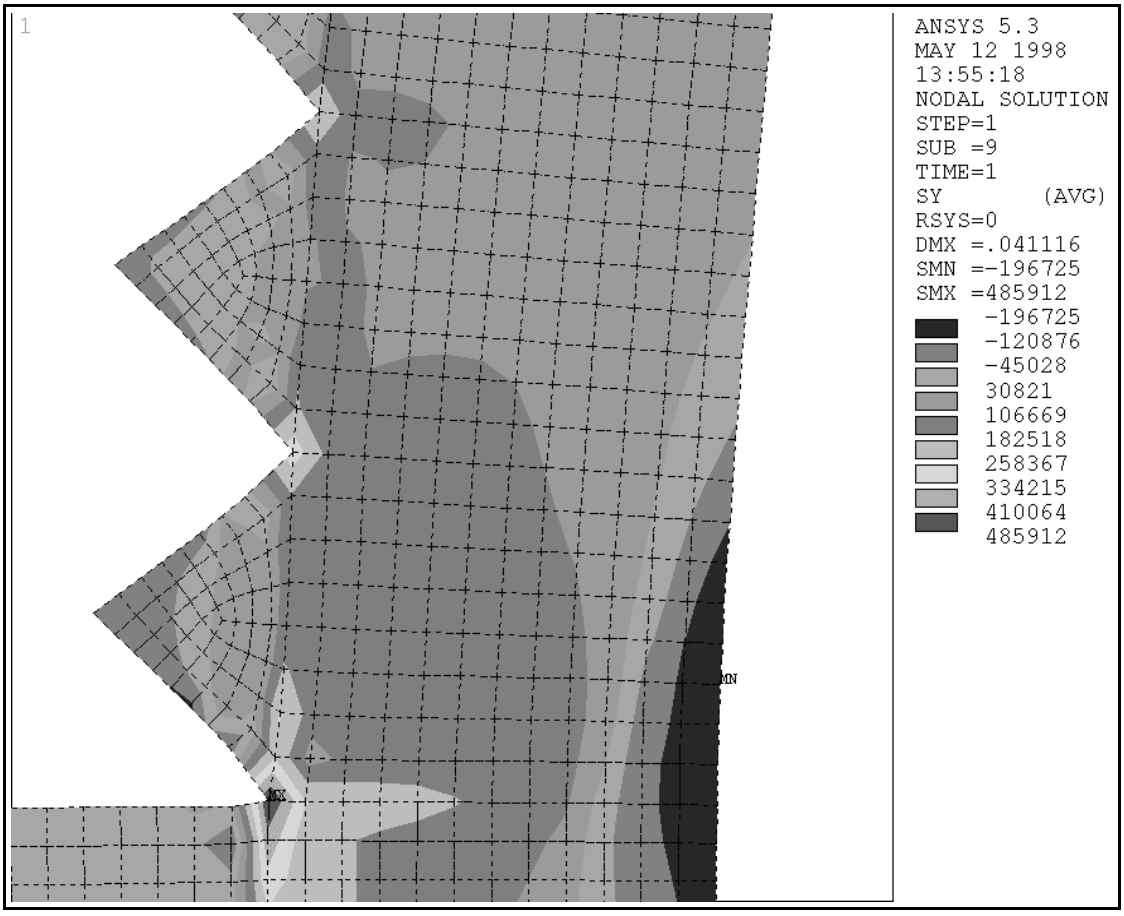

Fig. 6. Axial stress plot of ANSYS model (threaded region).

The FE model was constructed in ANSYS 5.3 using a fine density of 4-node quadrilateral axisymmetric elements. No contact forces were applied to the mating thread surfaces between the vessel and plug. However, upon observing the deflection animation between thread surfaces, it was observed that the radial expansion of the vessel created a gap between threads. This observation led to the manufacture of Specimen Lot B (discussed in Section 4), where the threads from the plug were removed, extinguishing any possibility of thread interaction.

Owing to the fact that this particular heat treatment (MHT) is nonstandard in the industry, two uniaxial tension specimens were procured for the characterization of the material, especially deep into the plastic zone of the stress–strain curve. After receipt of the uniaxial tension test results, the engineering stress–strain curve was converted to a true stress–strain curve through 30% strain (prior to necking). These data were input into ANSYS, and two load step sequences were created, accounting for an initial ramped pressure to 39,500 psi, and then a sudden depressurization to 0 psi. This type of loading was more typical of the actual test conditions, where diametric measurements took place with no applied pressure.

Using true stress–strain properties, and numerically enacting a simulated sudden depressurization, the nonlinear FE model produced radial deflections within 5% of the experimental data. The axial stress plots are shown in Figs. 5 and 6, where the stresses shown are resulting from an internal pressure of 39.5 ksi.

With the FE model radial deflections within acceptable limits, the axial stresses on the plug side of second thread root were reported to be 158.2 ksi (shown as the σ_{zz} locations in Fig. 7). Although stress values were much larger (263.3 ksi) near the root of the first thread, experimental failures occurred at the root of the second thread. It is theorized that the heat generated during the electron beam welding was sufficient to melt the first thread, thereby fusing it with surrounding material. Thereby, the welding process diminished the stress concentration at that location, along with locally annealing the material.

When comparing the predicted far-field stress value range of 147.3–164.6 ksi$\sqrt{\text{in.}}$ (based upon linear elastic fracture mechanics in Eq. (4)) with the axial stress of 158.2 ksi$\sqrt{\text{in.}}$ near (not directly at) the root of the second thread (obtained from FEA results using an applied pressure of 39.5 ksi), a good correlation between the two theoretical methods is observed.

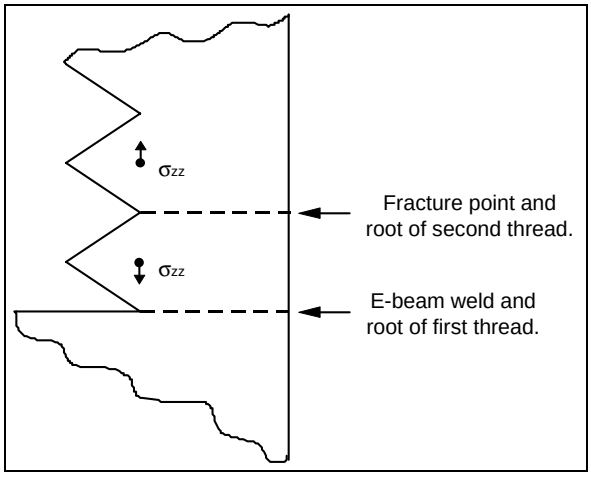

Fig. 7. Location of axial stress in FEA.

4. Experimental procedures

4.1. Specimen preparation

Two different lots of pressure vessel specimens were prepared as follows:

Lot A: Two 0.75 in. diameter solid blanks were machined within 0.01 in. of final dimensions, and then heat treated using the MHT specification. Following the heat treatment, the specimens were machined to their final dimensions, threaded to an Inconel X-750 plug, and finally electron-beam welded together according to the AMS 2681 specification [11].
Lot B: Three samples from Lot A were taken and welded to nonthreaded Inconel X-750 plugs.

Hence, upon comparing the lots, it will be noted that the presence, or absence, of threads on the weld plug is different. In both lots, post-heat-treatment machining was required to satisfy dimensional tolerances.

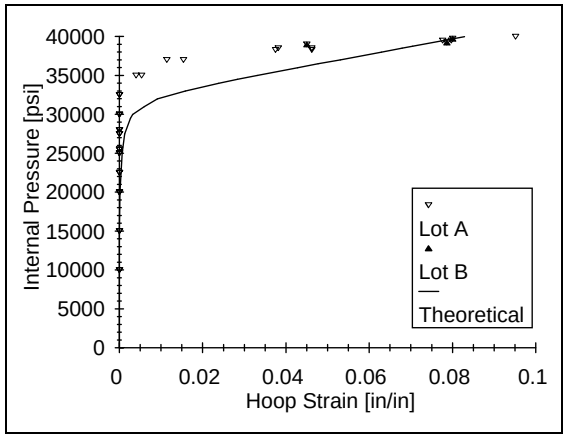

Fig. 8. Pressure–expansion curve for pressure vessel.

4.2. Pressure testing

Pressure testing of the specimens occurred in two experimental setups:

Test 1: The specimens from Lot A were attached to a pressure manifold, which was connected to a 40,000 psi handpump. Pressure was monitored with a Bourdon tube analog gauge, having an accuracy of ± 200 psi. First, the outside diameter on all specimens was initially measured. Then, incremental steps of pressure (5000 psi or less) were applied to the specimens, and, for safety reasons, the pressure was removed prior to remeasuring the specimens. When one specimen reached its rupture point, it was removed from the manifold and testing continued. This approach was taken until all specimens had ruptured.
Test 2: One specimen at a time from Lot B was attached to a dead weight tester capable of generating 50,000 psi. Pressure was slowly increased until rupture occurred. Pressure was controlled in 250 psi increments near the rupture point of the specimen. In this procedure, each specimen was pressurized to failure on an individual basis. No intermediate measurements were made: only initial and final measurements, along with the rupture pressures were obtained from this test. By this means, the effects of cyclic pressurization (as done in Test 1) were eliminated.

The radial deflections from the experiments were converted to hoop strains as follows [12]:

$$\varepsilon_{\theta\theta} = \frac{\Delta D}{D_o} = \left(\frac{\text{change in external diameter}}{\text{original external diameter}}\right). \quad (5)$$

5. Results and discussion

The residual pressure-expansion data from Lots A and B are shown in Fig. 8, along with a “Theoretical” line, which represents data obtained from the ANSYS 5.3 FEA.

A comparative photograph of test specimens is shown in Fig. 9. At the point of rupture, the fracture-induced crack

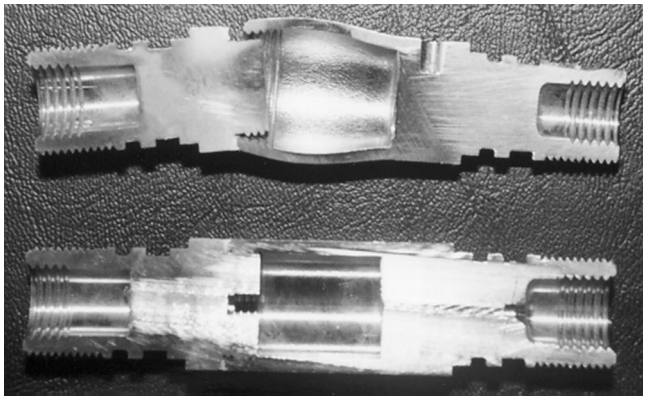

Fig. 9. Pressure vessel specimens: pre- and post-rupture pressure.

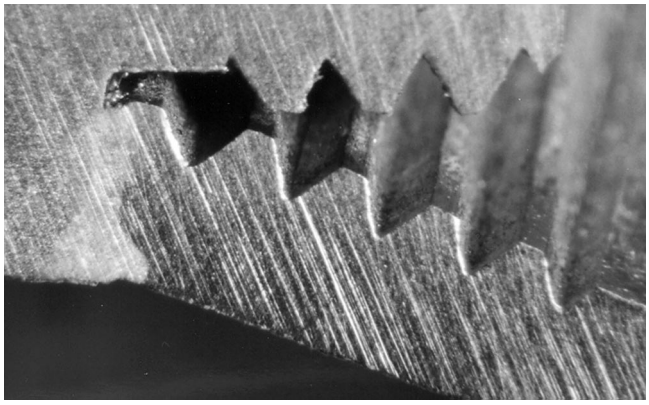

Fig. 10. View of deflected housing after rupture.

spread radially around 50–75% of the vessel circumference, generally following along the root of the second thread. One of the specimens from Lot A experienced a severe fracture, where the crack fully extended around the entire circumference, initiating a separation between vessel and plug.

Note in Fig. 10, the threads between vessel and plug have completely separated by the time the vessel ruptures. Removal of threads from the weld plugs in Lot B revealed no significant change in the measured rupture pressure. The rupture pressures between Lot A and Lot B were within 1.3%. Also note that the electron-beam weld has virtually consumed (melted) the first thread root, thus rendering the second thread root the most likely point of fracture.

In Fig. 11, a magnified view of the fracture is shown. Note the angle of the left hand side fractured surface is nearly vertical, indicating a sudden, brittle-type, failure. The left hand side fracture surface does, however, indicate some minor plasticity taking place, as seen by the mild resemblance of a "cup and cone" fracture.

The results in Table 1 indicate experimental pressures and hoop strains, and the theoretical hoop strains based upon the experimental rupture pressure. Experimental values are averages, shown with uncertainties calculated as the standard deviation.

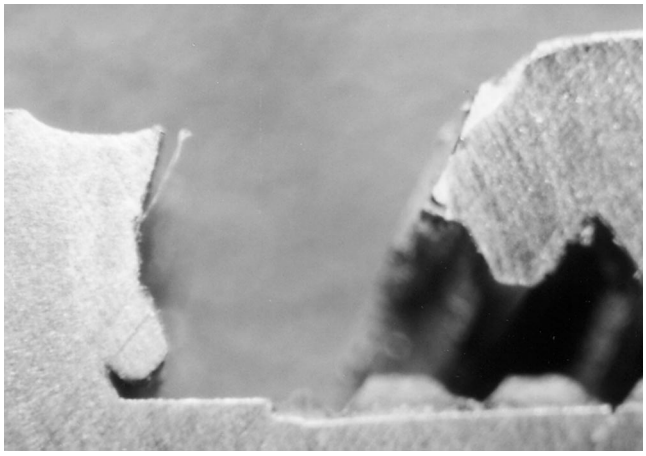

Fig. 11. Magnified view of a fracture point.

One specimen from Lot B exhibited a significantly smaller deflection at rupture ($\varepsilon_{\theta\theta} = 0.0450$ at 39,000 psi). Based upon Chauvenet's criterion [13], it is permissible to reject the point, but it has been included both in Fig. 8 and in Table 1. It is believed that this particular specimen fractured prior to reaching the instability point where bulging begins.

6. Conclusions

In the design of welded high pressure vessels, a threaded joint often exists between parts. The presence of such threads introduces stress risers, which may lead to the nucleation of crack emanating from the root of a thread. Thus, the subject of eventual concern is to see if one can predict the critical internal pressure, which may lead to the catastrophic failure of the vessel.

Using this approach, a combination of fracture mechanics and nonlinear FEA is required to estimate the rupture pressure of a threaded pressure vessel. First, the far-field stress is obtained from linear-elastic fracture mechanics (LEFM). Second, an axisymmetric FE model is generated, to which various pressures are numerically applied.

For the analysis, two correction factors are applicable in determining the far-field stress from the value of the material fracture toughness. The first correction factor approximates the internal thread of the pressure vessel as an edge crack in a flat plate (Eq. (2)). The second correction factor accounts for the cylindrical geometry of the vessel (Eq. (3)). Combined together, an estimate of the far-field stress is easily obtained, assuming that a valid plane strain fracture toughness value K_{Ic} for the material has been established. Ideally, this material property should be obtained from tests carried out on specimens, which have been processed in the similar manner, as the actual component will be. Furthermore, the fracture toughness value should also be representative of the thickness of the specimen.

The FEA axial stress near the root of the threads (see

Table 1
A comparison of hoop strains derived from various methods

Solution type	Pressure (ksi)	Hoop strain, $\varepsilon_{\theta\theta}$ (in./in.)	Comments
Experimental	39.8 ± 0.4	0.0868 ± 0.0118	Lot A (2 samples)
	39.3 ± 0.4	0.0677 ± 0.0196	Lot B (3 samples)
	39.5 ± 0.4	0.0794 ± 0.0004	Lot B (2 samples)[a]
	39.5 ± 0.4	0.0754 ± 0.0185	Lots A & B (5 samples)
	39.6 ± 0.3	0.0829 ± 0.0092	Lots A & B (4 samples)[a]
Linear elastic	39.5	0.0044	
Nonlinear elasto-plastic (ANSYS 5.3)	39.5, unload to 0	0.0886, 0.0830	True σ–ε curve

[a] By Chauvenet's criterion, one sample has been rejected.

Fig. 7) is examined and compared to the far-field stress (obtained from LEFM). During the finite element analysis, iterative changes to the numerically applied pressure are required, until the two stresses compare favorably, thus deriving an estimate of the critical pressure required to fracture the vessel. The FE model should be refined to determine that the solution is converging. Great care should also be exercised to use the true stress–strain properties which represent the material in its "as-processed" state.

Experimental tests correlated very well with this analytical approach, not only with the theoretical rupture pressure of the vessel, but also with the amount of permanent hoop strain after fracture, as predicted by the finite element analysis.

References

[1] Shigley JE, Mischke CR. Mechanical engineering design, San Francisco: McGraw-Hill, 1989 p. 59.
[2] Popov Egor P. Engineering mechanics of solids, New Jersey: Prentice Hall, 1990 pp. 165–169.
[3] Griffith AA. The phenomenon of rupture and flow in solids. Philosophical Transactions, Series A 1920;221:163–198.
[4] Williams ML. Stress singularities at the tip of a wedge. J Appl Mech 1952;19:526.
[5] Broek D. Elementary engineering fracture mechanics, Boston: Kluwer Academic, 1991 p. 85.
[6] Folias ES. A circumferential crack in a pressurized cylindrical shell. Int J Fracture Mech 1967;3-1:1–12.
[7] Anderson TL. Fracture mechanics—fundamentals and applications, Michigan: CRC Press, 1995 p. 87.
[8] Metals Handbook. 10th Edition, American Society for Metals, vol. 4, 1991, pp. 804–807.
[9] Mills WJ. Effect of heat treatment on the tensile and fracture toughness behavior of alloy 718 weldments. Welding Research Supplement 1984;237–245.
[10] Mills WJ. Fracture toughness variations for alloy 718 base metal and welds, superalloy 718—metallurgy and applications. The Minerals, Metals, and Materials Society 1989:517–532.
[11] Society of Automotive Engineers, AMS 2681A: Electron Beam Welding. Pennsylvania, 1 January, 1992.
[12] Johnson W, Mellor PB. Engineering plasticity, New York: Halsted Press, 1983 p. 226.
[13] Taylor JR. An introduction to error analysis, California: University Science Books, 1982 pp. 142–144.